Available online at www.sciencedirect.com
ScienceDirect
Polymer 48 (2007) 371–381
polymer
www.elsevier.com/locate/polymer

Miscibility and mechanical properties of quaternized polysulfone/benzoyl guar gum blends

Yihong Huang, Chaobo Xiao*

College of Chemistry and Molecular Sciences, Wuhan University, Wuhan 430072, People's Republic of China

Received 20 August 2006; received in revised form 29 October 2006; accepted 31 October 2006
Available online 27 November 2006

Abstract

Novel blends from quaternized polysulfone (QPSF) and benzoyl guar gum (BGG) coded as QB with different contents (10–80 wt%) were prepared through solution casting method. Simultaneously, other kinds of blends were prepared from chloromethylated polysulfone (ClPSF) and BGG coded as ClB to compare the effects of the substituted groups on the miscibility and properties of the composite materials. The effect of BGG content on QB blends was investigated by Fourier transform infrared spectroscopy (FTIR), scanning electron microscopy (SEM), atom force microscopy (AFM), differential scanning calorimetry (DSC) and tensile tests. The results revealed that QB blends had good or certain miscibility over the entire composition ratio of BGG to QPSF under study. Compared with ClB blends, QB blends exhibited stronger interfacial attraction and better phase mixing as a result of the relatively strong hydrogen bonding and the specific electrostatic interaction between QPSF and BGG. The occurrence of strong interaction between QPSF and BGG played a key role in improving the material performance. With an increase of BGG content in the blends, the tensile strength of QB blends increased from 33.1 to 44.3 MPa. Furthermore, the mechanical properties of QB-20 blend at different RH were also discussed. It was found that the composite properties changed considerably with moisture content, which attributed that water molecules had a great effect on the hydrogen bonding between the two polymers.

Keywords: Quaternized polysulfone; Benzoyl guar gum; Miscibility

1. Introduction

Recently, the bad environmental situation caused by overburdensome pollutants presses for advancement of materials from renewable resources, which has the potential to substitute for some petrochemical products [1]. Among several candidates including natural polysaccharides and their derivatives, guar gum (GG), a high-molecular weight water-soluble non-ionic natural polysaccharide isolated from the seed endosperm of the guar plant, is one of the promising materials for biodegradable plastics because it is a versatile biopolymer with immense potential and low price for use in the non-food industries [2]. It is a member of the class of galactomannans, which consist of a (1,4)-linked β-D-mannopyranosyl backbone partially substituted at O-6 with α-D-galactopyranosyl side groups [3]. Abundant hydroxyl groups in natural polysaccharides facilitate the formation of hydrogen bonding with other polymers, which causes natural polysaccharides miscible with synthetic polymers [4–6]. However, most of the natural polysaccharides exhibit unusually high water absorbency, absence of peculiar functionalities and fast biodegradability, which limit its use to a certain extent. By replacing the hydrogen atoms of the hydroxyl groups with others groups, natural polysaccharide derivatives such as benzyl konjac glucomannan, benzyl starch, nitrolignin, cellulose acetate and nitrocellulose, have widely been applied to improve the mechanical strength of polyurethane [7–11].

Polysulfone (PSF), because of its excellent properties such as mechanical, thermal and chemical stabilities, has been most

* Corresponding author.
E-mail address: cbxiao@whu.edu.cn (C. Xiao).

0032-3861/$ - see front matter © 2006 Elsevier Ltd. All rights reserved.
doi:10.1016/j.polymer.2006.10.041

widely used in the manufacture of synthetic polymer membranes [12,13]. To improve the mechanical properties and fouling, many papers have reported the blends between polysulfone and other synthetic polymers such as polyamide 6, poly(acrylic acid), rubber, cyanate ester resin, poly(vinyl alcohol), poly(ethylene-octene), polysiloxan, polyvinylpyrrolidone, etc [14–21]. However, owing to the lack of the specific interactions in the two polymers, there is scarce miscibility in the above blends. In order to improve the miscibility and compatibility, some authors have begun to modify the polysulfone by introducing specific functional groups to the polymers. According to the reports by Deimede et al. [22], sulfonation of polysulfone resulted in polar groups in the main chain, which were miscible with polybenzimidazole.

Polymer blends continue to be a subject of intense investigation because of its simplicity and effectiveness of mixing two different polymers to produce new materials, from both academic and industrial views, in the last decades [23]. The development of new useful blends is severely limited by the complete incompatibility of many polymer pairs of interest [24]. Because of the very small contribution from the entropy of mixing, it is difficult to obtain miscible compositions of two high molecular weight polymers. One way to overcome this drawback is the development of specific interactions such as hydrogen bonding, electrostatic interaction, ion–dipole and charge transfer by introducing specific functional groups to the polymers. Several studies have been carried out concerning the miscibility behavior of polymers bearing polar groups and polyamides [25,26].

The blends from polysulfone or modified polysulfone and natural polymers have been scarcely reported. A basic understanding of the behavior for QPSF/BGG blends is essential for a successful research and development of the novel biodegradable polysulfone-based materials. So, in this study, quaternized polysulfone was synthesized and then blended with BGG through solution casting method. The effect of BGG content on the miscibility, morphology and physical properties of the resulting blends was also investigated by FTIR, SEM, AFM, DSC and measurements of mechanical properties.

2. Experimental

2.1. Materials

Guar gum was kindly supplied by Wuhan Tianyuan Biology Co., China. The method of preparation and purification is followed as described earlier [27]. Polysulfone (UDEL, $M_w = 5.1 \times 10^4$) was obtained from Solvay Chemical Company Inc. and dried in vacuum at 60 °C before use. Paraformaldehyde, chlorotrimethylsilane and benzoyl chloride were purchased from Aldrich Chemical Company Inc., and used as received without further purification. *N*,*N*-dimethylformamide (DMF) was purchased from Shanghai Chemical Company Inc., and dried over molecular sieves before use. The other reagents were used without further purification.

2.2. Synthesis of quaternized polysulfone

Chloromethylated polysulfone was prepared using the report by Avram [28]. The chloromethylation reaction occurs according to Scheme 1. Polysulfone 10 g (22.6 mmol) was dissolved in 350 ml 1,2-dichloroethane. The solution was heated to 50–55 °C, then 6.78 g (226 mmol) paraformaldehyde, 24.60 g (226 mmol) chlorotrimethylsilane and 0.59 g (2.3 mmol) $SnCl_4$ were added. The mixture of commercial paraformaldehyde/chlorotrimethylsilane ($ClSiMe_3$) as chloromethylation agent and $SnCl_4$ as catalyst were used for the chloromethylation reaction of polysulfone. Reaction time was varied from 2 to 72 h in order to obtain different degrees of substitution (DS) of chloromethylated products. Once the reaction time was completed, the reaction mixture poured into hot water to evaporate 1,2-dichloroethane out. At last, the white product was dissolved several times in DMF and reprecipitated in water for removing excess paraformaldehyde, chlorotrimethylsilane and $SnCl_4$. The resulting product was air-dried and dried at 50 °C in vacuo. The characteristics of the chloromethylated polysulfone are given in Table 1. The total chlorine content of chloromethylated polysulfones was determined by a Schöniger method [29]. The degree of substitution (DS) was calculated using the following equation:

$$\mathrm{DS} = \frac{M_{\mathrm{PSF}}\ c_{\mathrm{Cl}}}{M_{\mathrm{Cl}}100 - M_{\mathrm{CH_2Cl}}\ c_{\mathrm{Cl}}} \quad (1)$$

Where, M_{PSF}, M_{Cl}, $M_{\mathrm{CH_2Cl}}$ and c_{Cl}, are referred to molecular weight of structural unit of PSF, atomic weight of chlorine, molecular weight of CH_2Cl group and concentration of chlorine analytically determined, respectively.

In this work, the method of quaternization is different from the traditional literature. In the traditional method, ClPSF was immersed into trimethylamine aqueous solution to complete the quaternization process, which was a kind of typical gas–solid reaction. Compared with the gas–liquid reaction,

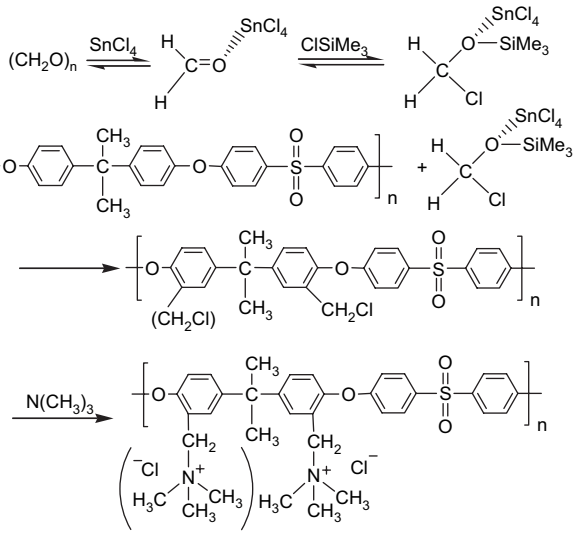

Scheme 1. Reaction scheme for the synthesis of ClPSF and QPSF.

Table 1
Characteristics of the chloromethylated polysulfone

Samples	DS[a]	M_w[b]	M_w/M_n	T_g[c] (°C)	T_{50}[d] (wt%)
ClPSF-0.35	0.35	5.02×10^4	2.68	194.3	578
ClPSF-0.49	0.49	4.85×10^4	2.73	186.9	569
ClPSF-0.86	0.86	4.96×10^4	2.81	184.3	563
ClPSF-1.01	1.01	5.21×10^4	2.80	183.1	556
ClPSF-1.36	1.36	5.34×10^4	2.95	175.2	543
ClPSF-1.71	1.71	5.30×10^4	2.96	169.4	533

[a] Substitution degree was calculated from the chlorine content determined by using a Schöniger method.
[b] Weight-average molecular weight (M_w) was determined with a multiangle laser light scattering methods.
[c] Glass transition temperature from DSC measurements (second heating cycle, heating rate 20 °C min^{-1}, heating range between 50 and 250 °C).
[d] Temperature from TGA measurements corresponding to 50 wt% loss.

Table 2
Characteristics of the quaternized polysulfone

Samples	DS[a]	M_w[b]	M_w/M_n	T_g[c] (°C)	T_{50}[d] (wt%)
QPSF-0.35	0.38	5.21×10^4	2.65	195.8	511
QPSF-0.49	0.51	5.14×10^4	2.76	191.4	503
QPSF-0.86	0.86	5.42×10^4	2.83	189.5	491
QPSF-1.01	0.98	5.78×10^4	2.79	187.9	486
QPSF-1.36	1.32	6.09×10^4	2.87	183.3	478
QPSF-1.71	1.69	6.25×10^4	2.91	175.3	474

[a] Substitution degree was determined by the content in ionic chlorine, which can be titrated with 0.02 mol/l aqueous $AgNO_3$ solution.
[b] Weight-average molecular weight (M_w) was determined with a multiangle laser light scattering methods.
[c] Glass transition temperature from DSC measurements (second heating cycle, heating rate 10 °C min^{-1}, heating range between 50 and 280 °C).
[d] Temperature from TGA measurements corresponding to 50 wt% loss.

gas–solid reaction requires higher activation energy, which has greatly limited effective quaternization. Furthermore, the low concentration of trimethylamine in the aqueous solution will also result in an incomplete quaternization. Some chloromethylated groups in polysulfone chain cannot be quaternized completely, which cause a dissymmetrical structure in QPSF structures. Now, there is an improved method to quaternize ClPSF effectively and simply. The method is as follows: ClPSF was dissolved in DMF in a subuliform flask equipped with a magnetic stirrer and a long pipe. Then trimethylamine aqueous solution was put into a three-necked round flask equipped with a magnetic stirrer, a safe flask and a long pipe. Through a round $CaCl_2$ desiccator, the two pipes were linked together. Then trimethylamine solution was heated slowly to evaporate out trimethylamine gas. The gas was dried through $CaCl_2$ desiccator and piped into ClPSF solution. After a few minutes, the buff ClPSF solution was converted into deeply yellow QPSF solution. The reaction of quaternization happened in gas–liquid media while not in gas–solid media. Obviously, QPSF should have a symmetry structure. The quaternary polymers were isolated from the reaction medium by precipitation in diethylether, washed several times with diethylether, and dried for several days under a vacuum at room temperature. The DS of quaternized PSF is determined by the content in ionic chlorine, which can be titrated with 0.02 mol/l aqueous $AgNO_3$ solution. The equation was as followed:

$$\mathrm{DS} = \frac{M_{\mathrm{PSF}}\left(c_{\mathrm{AgNO_3}} V_{\mathrm{AgNO_3}}\right)}{100 - M_{\mathrm{N(CH_3)_3Cl}}\left(c_{\mathrm{AgNO_3}} V_{\mathrm{AgNO_3}}\right)} \quad (2)$$

Where, M_{PSF}, $c_{\mathrm{AgNO_3}}$, $V_{\mathrm{AgNO_3}}$, and $M_{\mathrm{N(CH_3)_3Cl}}$, are referred to the molecular weight of structural unit of PSF, concentrations of $AgNO_3$ solution, total titrated amount of $AgNO_3$ solution and molecular weight of $-N(CH_3)_3Cl$ group, respectively. The corresponding characteristics of QPSF are given in Table 2. We can see that the substitution degree of QPSF is good fit to the value of ClPSF, which indicated that ClPSF is completely quaternized by the gas-piping method.

FTIR spectra of the PSF, ClPSF and QPSF blends are shown in Fig. 1. Compared with PSF, the band at 760 cm^{-1} is attributed to the C–Cl absorption. After quaternization, two new peaks appeared in QPSF at 975 and 921 cm^{-1}, which are attributed to the C–N absorption stretching. This indicates that ClPSF and QPSF have been synthesized successfully.

2.3. Preparation of BGG

The preparation of benzoyl guar gum was as follows: 2.0 g guar gum was dissolved in 200.0 ml water and then was put into a three-necked flask equipped with a mechanical stirrer, a dropping funnel and a condenser. The flask was stirred vigorously and 50 ml of 40 wt% aqueous NaOH solution was added dropwise. The resulting alkali-guar gum slurry was stirred at 40 °C for 2 h before the dropwise addition of 25 ml of benzoyl chloride. The reaction was performed at

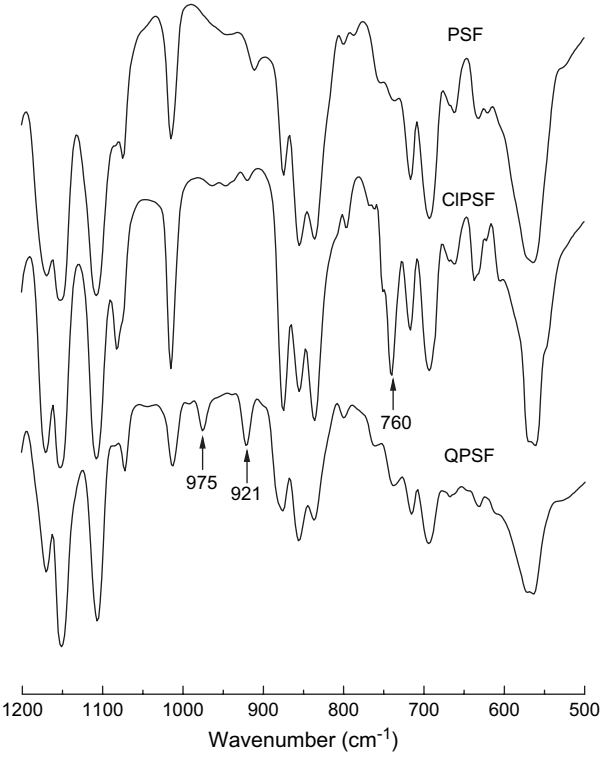

Fig. 1. FTIR spectra of the PSF, ClPSF and QPSF sample.

ice-water bath for 2 h, and a white product was obtained as a precipitate. This crude precipitate was dissolved with DMF and then precipitated and washed several times with water. After vacuum drying at 50 °C, the white powder of BGG was obtained. The reaction process is represented in Scheme 2. The FTIR spectra of the GG and BGG are shown in Fig. 2. The broad stretching band of −OH groups at around 3994 cm^{-1} sharply decreases in the spectrum of BGG, and this indicates that some hydrogen atoms of −OH groups in guar gum are substituted by benzoyl groups. Moreover, the spectrum of BGG shows characteristic aromatic stretching at 1450, 1580 and 1600 cm^{-1}. The band at 1725 cm^{-1} is attributed to the stretching of −C═O, while the C−H aromatic stretching is located at 3030 cm^{-1}. These indicate that BGG has been synthesized successfully. The degree of substitution is calculated to be 1.3 from elemental data obtained with a CHN−O Rapid elemental analyzer (Heraeus Co., Germany) according to Ref. [30]. The weight-average molecular weight of BGG is determined with a multiangle laser light scattering instrument to be 3.12×10^5 and its polydispersity index (M_w/M_n) was 1.41.

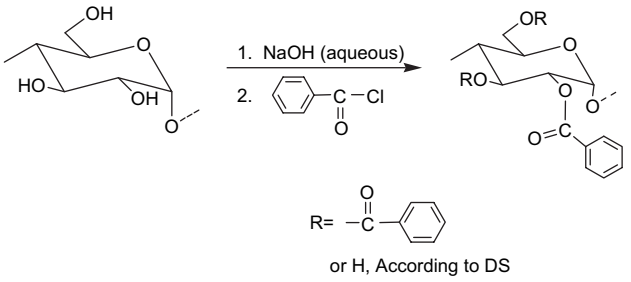

Scheme 2. Reaction scheme for the preparation of BGG.

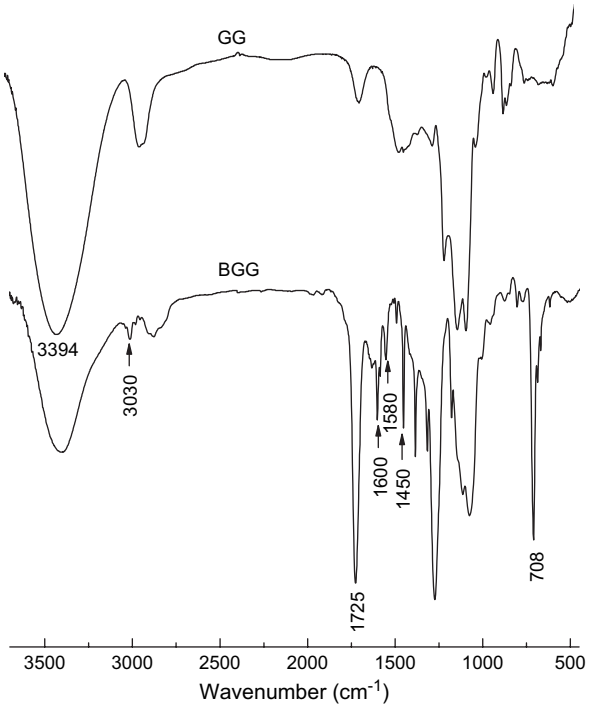

Fig. 2. FTIR spectra of the GG and BGG sample.

2.4. Preparation of the blends

When the DS value was less than 0.35, QPSF was immiscible with BGG, which was resulted from the lack of enough quaternized groups in the aromatic rings. In this work, without special illumination, the DS value of QPSF in the QB blends was 0.98. We believe that QPSF in possession of high DS will be miscible with BGG. QPSF and BGG were dissolved in DMF to obtain 10 wt% concentrated solution. Subsequently, QPSF solution was mixed with varying amounts of BGG solution at room temperature with continuous stirring for 2 h. Finally, the mixture was degassed and then cast on a glass plate mold, followed by drying at 80 °C in an oven for two days to obtain a transparent blend. By changing the weight percent of BGG in the blends such as 10, 20, 40, 50, 60 and 80 wt%, a series of blends were prepared, coded as QB-10, QB-20, QB-40, QB-50, QB-60 and QB-80, respectively. The blends from pure QPSF and BGG were coded as QPSF and BGG, respectively. Simultaneously, another blends prepared from chloromethylated polysulfone (ClPSF) and BGG coded as ClB were also followed with the above methods. By changing the weight percent of BGG in the blends such as 10, 20, 40, 50, 60 and 80 wt%, a series of blends were prepared, coded as ClB-10, ClB-20, ClB-40, ClB-50, ClB-60 and ClB-80, respectively. The blend from pure ClPSF was coded as ClPSF. The thickness of the two series of blends was controlled to be about 0.1 mm. All the blends were vacuum-dried at room temperature for three days and kept in a desiccator with P_2O_5 as a desiccant for more than one week before the characterization. In the tensile tests, the moisture content of the QB blends was achieved by conditioning the samples at room temperature in desiccator containing saturated $Mg(NO_3)_2 \cdot 6H_2O$ solution to provide a relative humidity (RH) of 52%.

2.5. Characterization

Static multiangle laser light scattering instrument (SMLLS) was equipped with a He−Ne laser (DAWN-DSP, Wyatt Technology Co., USA) in the angle range from 42° to 136° at 25 °C. Refractive index increment (d*n*/d*c*) was measured with a double-beam-differential refractometer (DRM-1020, Otsuka Electronic Co., Japan) at 25 °C and 632.8 nm. All solutions were filtered with a sand filter and then with 0.45 mm filter (DTFE, Puradisce 13 mm Syringe Filter, Whattman, England). Astra software was utilized for the data acquisition and analysis.

FTIR spectra of the blends were taken on a Nicolet 170SX FTIR spectrometer in a wave number range 4000−400 cm^{-1}. The blends were cut to powder and then mixed with potassium bromide to laminate.

SEM micrographs were taken on a Hitachi S-570 microscope (Japan). The blends were snapped and the cross-section of the blends was sputtered with gold, observed, and photographed.

AFM analyses were prepared by dissolving 10 mg of the blends in 1 ml of DMF and then spin casting a 50 ml aliquot of the polymer mixture solution onto a freshly cleaved 1 cm × 1 cm square mica substrate at 1000 rpm. The samples were dried at 60 °C in an oven for 0.5 h before analysis. The blends were generated with QB-40 and QB-80 samples. AFM measurements were performed on a Picoscan atomic force microscope (Molecular Imaging, United States) in a MAC mode with commercial MAC lever II tips (Molecular Imaging, United States), with a spring constant of 0.95 N m^{-1}. The measurements were performed in air at ambient pressure and humidity and the images were stored as 256 × 256 point arrays.

DSC thermograms over the temperature range 50–280 °C were determined using a differential scanning calorimeter (TA2920, USA). Each sample conditioned at 52% RH was subjected to the heating/cooling cycle between 50 and 280 °C with a scanning rate of 10 °C/min to obtain the reproducible glass transition temperature (T_g) values. For a polymer, T_g was taken at the half-variation in heat capacity occurring at the glass–rubber transition. Scanning rate in the second run was 10 °C/min.

WAXD patterns of the blends were recorded on a WAXD instrument (XRD-6000, Shimadzu, Japan) with Cu Kα radiation (wavelength = 0.1542 × 10^{-10} m) at 40 kV and 30 mA, and the samples were examined with 2θ values of 5–40° at a scanning rate of 4° per minute.

Tensile tests of the blends were measured on a universal testing machine (CMT6502, Shenzhen SANS Test Machine Co. Ltd., China) with a tensile rate of 5 mm/min^{-1} according to ISO6239-1986 (E') to obtain tensile strength and elongation at break. The mean values of tensile strength and elongation at break were obtained from five replications.

The moisture content was achieved by conditioning the samples at room temperature in desiccator containing saturated inorganic salts solution to provide a relative humidity (RH). The saturated salt solutions were P_2O_5, $ZnCl_2$, CH_3COOK, $CaCl_2 \cdot 6H_2O$, $Zn(NO_3)_2 \cdot 6H_2O$, $Mg(NO_3)_2 \cdot 6H_2O$, $NaNO_2 \cdot 2H_2O$, $NaClO_3$, $KHSO_4$ and $CuSO_4 \cdot 5H_2O$. Conditioning was carried out for at least two weeks to ensure the equilibration. Then the equilibrated blends were measured on a universal testing machine.

3. Results and discussion

3.1. Structure and morphology of the blends

FTIR spectrometry has been proven to be a very powerful technique to detect the intermolecular interaction between two polymers. The FTIR hydroxyl stretching range of QPSF/BGG blends is sensitive to the hydrogen bonding formation. Fig. 3 illustrates FTIR spectra of all samples in the range 4000–2500 cm^{-1}. The band at 3410 cm^{-1} is attributed to the hydroxyl stretching in the blends. Interestingly, it is clear that a shoulder at 3280 cm^{-1} is assignable to vibration of the hydrogen bonding hydroxyl group. It proves that hydrogen bonding is created between QPSF and BGG, which causes

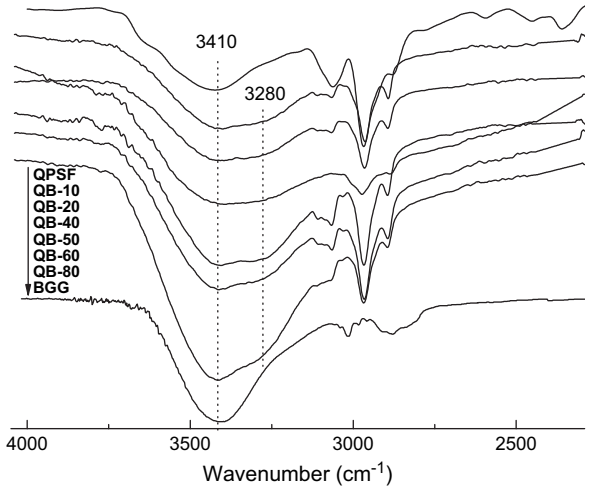

Fig. 3. FTIR spectra of the QB blends in the –OH region (4000–2500 cm^{-1}).

miscibility between the two polymers, and improves the physical properties of the blends. FTIR spectra of the blends in the C–O–C region are shown in Fig. 4. The band at 1053–1063 cm^{-1} is attributed to the C–O–C stretching vibration of BGG molecular structure. Compared with pure BGG, the band of C–O–C shifts increasingly to higher wave numbers with an increase of QPSF content in the blends. This effect is a consequence of changes in electronic distribution in the molecular structure of BGG resulting from the strong electrostatic interaction with quaternized groups [27].

SEM images of the ClB blends are shown in Fig. 5. The SEM photographs of cross-section of the investigated samples exhibit different structures. It can be seen that pure ClPSF and BGG exhibit smooth and homogeneous structure. For ClB-20 blend, it is possible to observe a nucleating structure resulting from aggregation of smaller nuclei in the ClPSF matrix, which indicates partial miscibility between ClPSF and BGG or good dispersion of BGG phase in ClPSF matrix. With an increase of BGG content, there are plenty of particles in the cross-section of ClB-40 blend, which explained that a small amount of BGG particles are dispersed in the continuous ClPSF matrix. It is

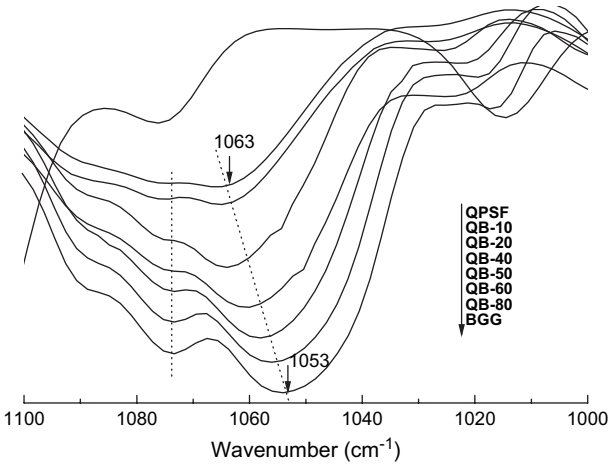

Fig. 4. FTIR spectra of the QB blends in the C–O–C region (1100–1000 cm^{-1}).

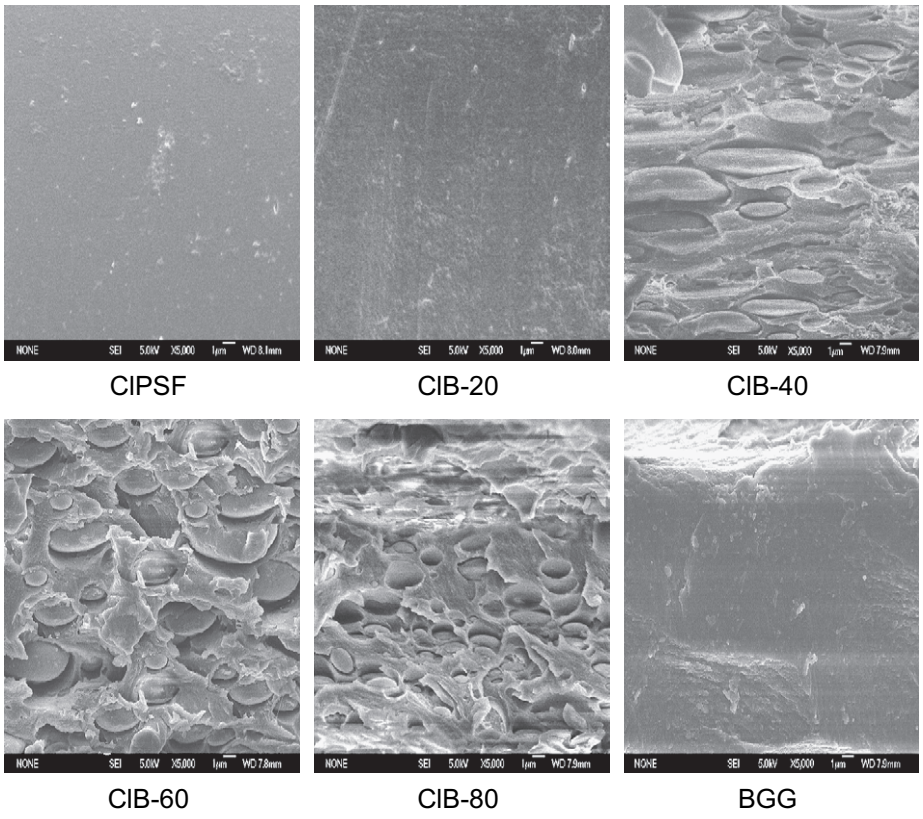

Fig. 5. SEM images of cross-sections of the ClB blends.

indicative of phase-separated polymer blend to some extent. When BGG content exceeds 50 wt%, BGG forms a continuous phase matrix and ClPSF as a dispersed phase. In ClB-60 blend, the big ellipsoid ClPSF particles are dispersed into BGG matrix, which indicates a serious phase separation in the blends. When BGG content further increases, BGG continues to control the phase behavior and the relatively small ClPSF particles are embedded into BGG matrix. From the SEM analysis, it can be concluded that there was lack of specific interactions between ClPSF and BGG, which leads to the serious phase separation.

Observation of the cross-sections of the fractured QB blends is illustrated in Fig. 6. QPSF displays a homogeneous morphology. When BGG content reaches 20 wt%, QB-20 blend exhibits coarse and fluctuant fracture surface, which indicates BGG is separated into QPSF matrix well. When BGG content further increases, we can observe the more compact structure in QB-40 blend, which is different from obvious phase separation in ClB-40 blend. It is believed that the quaternized groups on the PSF molecular chains can be helpful to improve the compatibility between PSF and BGG. There is a brittle and homogeneous fracture surface in QB-60 blend, which shows that a compatible one-phase system can be obtained. By comparison, the morphologies of QB-80 are quite different. The fracture zone appears to extend well beneath mechanism from that of the compatible composite materials [31]. In the later analyses, we can see dense structure in the AFM and only single T_g in the DSC, indicating QB-80 blend is miscible and compatible. From the SEM analysis, compared with the morphology of ClPSF/BGG blends, QPSF/BGG blends exhibit dense and homogeneous structure, owing that the strong interaction such as hydrogen bonding and electrostatic interaction between QPSF and BGG has improved the structure inside the blends and led to better component compatibility.

AFM micrographs of QB-40 and QB-80 are shown in Fig. 7. From the AFM, we can observe the compact structure in the blends, and a good miscibility is expected between QPSF and BGG. Compared with QB-40 blend, QB-80 blend exhibits more dense and compact structure, which implies that there is more strong interaction between the two polymers with an increase of BGG content. The molecular interaction in such a structure should be reflected in predictable improved performance of the blend materials.

3.2. Miscibility between QPSF and BGG in the blends

3.2.1. DSC analysis

The measurement of the glass transition temperature (T_g) of a polymer blend is often used as a criterion to determine its miscibility [32]. A miscible polymer blend would exhibit a single transition between T_g of the two components. With increasing immiscibility there is a broadening of the transition, whereas an incompatible system would be marked by separate transitions of the polymer components in the blends [33].

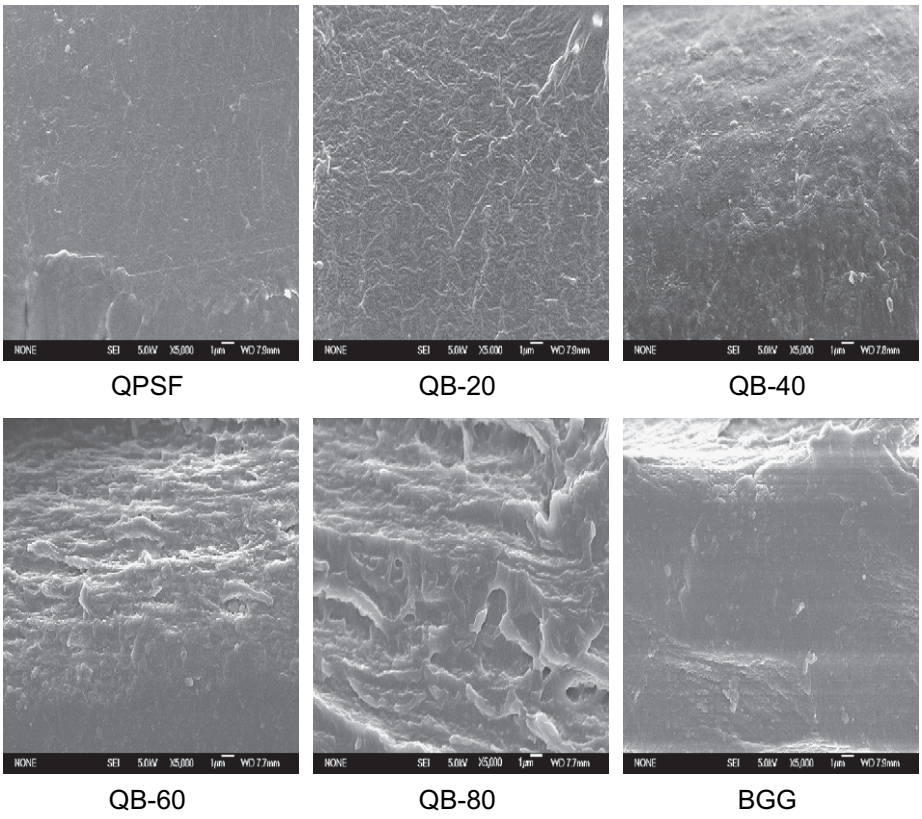

Fig. 6. SEM images of cross-section of the QB blends.

The DSC curves of the ClB blends are shown in Fig. 8, and the corresponding data of T_g are summarized in Table 3. The T_g of ClPSF and BGG are determined to be at 130.9 and 183.1 °C, respectively. For the blends with ClPSF content less than 20 wt%, one single T_g is observed, which shifts from 180.7 to 175.9 °C. This is an indication that the synergistic interaction occurs between ClPSF and BGG, which leads to a certain miscibility between ClPSF and BGG. With a further increase of BGG content, the resulting blends of ClB-40 and ClB-50 show two T_g transitions, corresponding to the phases of ClPSF and BGG, showing that phase separation occurs in the polymer blend. The observation of two T_g is in good agreement with the result from SEM analyses, which suggests that the blends are heterogeneous and the two starting components may fractionate into two different phases [34]. However, the divergence of two T_g in the blends is reduced compared

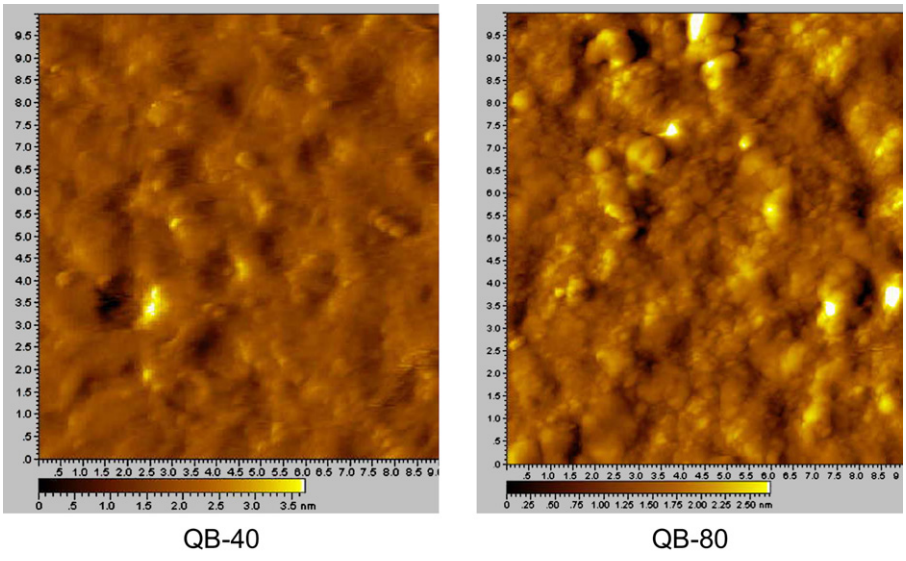

Fig. 7. AFM images of cross-section of QB-40 and QB-80 blends.

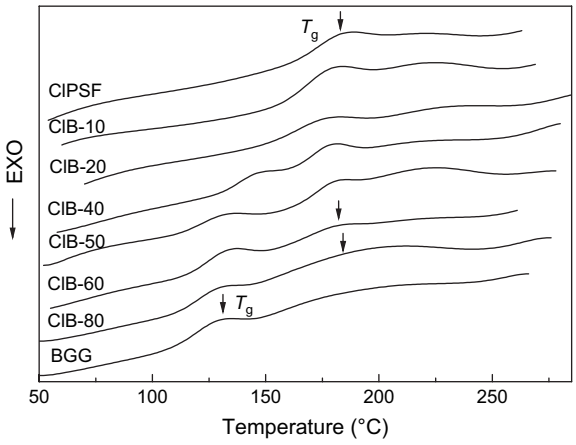

Fig. 8. DSC thermograms of the ClB blends.

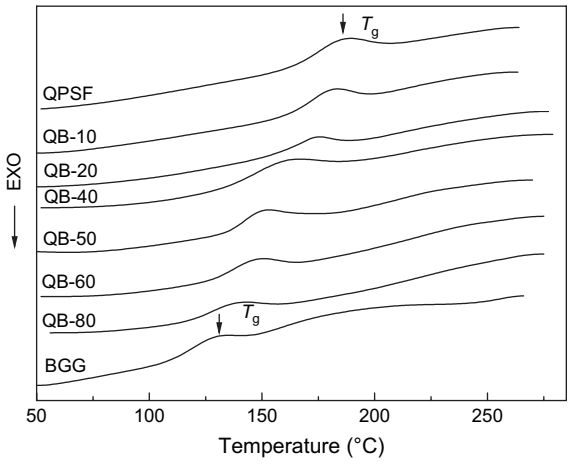

Fig. 9. DSC thermograms of the QB blends.

Table 3
Glass transition temperature of the ClB blends from DSC

Samples	BGG content (wt%)	Glass transition temperature (°C)	
		T_{g1}	T_{g2}
ClPSF	0	183.1	–
ClB-10	10	180.7	–
ClB-20	20	175.9	–
ClB-40	40	180.2	146.8
ClB-50	50	181.3	135.1
ClB-60	60	181.9	133.8
ClB-80	80	182.6	131.5
BGG	100	–	130.9

Table 4
Glass transition temperature of the QB blends from DSC

Samples	BGG content (wt%)	Glass transition temperature (T_g, °C)
QPSF	0	187.9
QB-10	10	180.6
QB-20	20	173.4
QB-40	40	159.5
QB-50	50	149.9
QB-60	60	146.1
QB-80	80	137.8
BGG	100	130.9

with that between pure ClPSF and BGG. Furthermore, with an increase of ClPSF content, T_{g2} shifts from 131.5 to 146.8 °C. This indicates that relatively weak interactions are taking place in the blends, leading to the mutual solubility between ClPSF and BGG. However, these interactions are not strong enough to ensure the miscibility of the blends with high content of BGG. A similar observation was also reported for the styrene-*co*-maleic anhydride random copolymers (SMA)/polyacrylate blends, which are immiscible when the content of maleic anhydride groups is lower than 8 wt% [35].

Fig. 9 shows DSC scans for the QPSF, BGG and QB blends with various BGG content, and the corresponding data are detailed in Table 4. The single T_g for each sample suggests that the blends have good or certain miscibility over the whole range of composition ratio. In addition, no endothermic peaks appear in the scans, indicating that crystalline regions do not exist in our samples. The DSC analysis also shows that the glass transition shifts to lower temperatures with an enhancement of BGG concentration. There are several classical equations that correlate the glass transition temperature of a miscible blend system with its composition [36–38]. These equations have been used to interpret both positive and negative deviations from the rule of mixtures, as well as S-shaped T_g vs composition curves. Fig. 10 shows the curve predicted from the T_g composition, which is obtained from Gordon–Taylor's equation [37]:

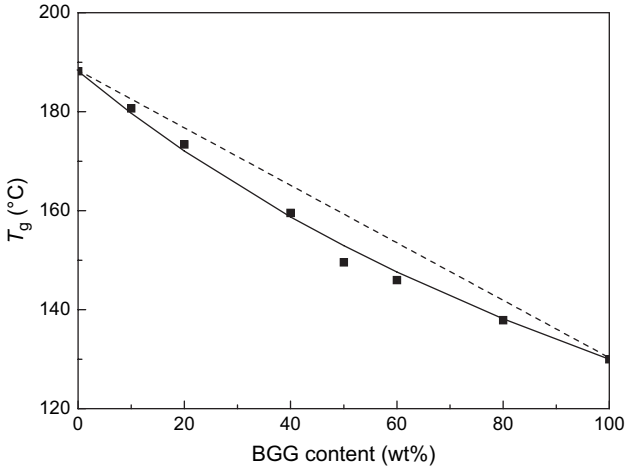

Fig. 10. Plot of T_g versus BGG content of the QB blends. The curves are those predicted by Gordon–Taylor's equation.

$$T_g = \frac{w_1 T_{g1} + k w_2 T_{g2}}{w_1 + k w_2} \tag{3}$$

where T_{g1}, T_{g2} and w_1, w_2 are the T_g's and weight fractions of components 1 and 2, respectively, T_g is the glass transition temperature of the blends, and k is an adjustable parameter ($k = 0.59$). Fig. 10 illustrates that Eq. (3) provides a good fit to the experimental data. The fit of Eq. (3) to the experimental

data offers good evidence for the miscibility of these blends. Prud'homme et al. have suggested that k can be taken as a semi-quantitative measure of strength for the interaction between the components of the blend [39,40]. For instance, in blends of poly(ε-caprolactone) with chlorinated polyethylene, poly(vinyl chloride) (PVC) and chlorinated PVC, k increases from 0.26 to 1.0. When such an approach is used for QPSF/BGG blends, a k value of 0.59 suggests a middle interaction between QPSF and BGG.

3.2.2. WAXD analysis

The measurement of the WAXD diffraction patterns of a polymer blend is also used as a criterion to determine its miscibility. If the two components have low compatibility then each polymer would have its own crystal region in the blend films, and the X-ray patterns of the samples would be expressed as simply mixed patterns of the two polymers with the same ratio as those for blending [41].

WAXD diffraction patterns of the ClB blends with different BGG contents are depicted in Fig. 11. All the blend compositions show a broad and diffuse peak, which indicates the amorphous nature of the blends. When BGG is introduced into the ClPSF matrix, the diffuse scattering peak near 18.2° (2θ), ascribed to ClPSF, have not apparently changed. When BGG content is less than 20 wt%, there is only a diffuse scattering observed in ClB-20 blend, indicating certain miscibility between ClPSF and BGG. As BGG content further increases, it is observed that there are two new diffuse scattering peaks near 6.5°and 22.6°, ascribed to BGG, appeared in the blends. This indicates that phase separation existed in the blends. In spite of phase separation, the broad intense peak in all the blends in comparison to the pure polymers indicates the presence of an ordered structure of the coexisting phases, which is also supported by the SEM and DSC.

WAXD patterns of the QPSF/BGG blends are different from ClPSF/BGG. Fig. 12 shows WAXD diffraction patterns of the QB blends. Compared with the ClB blends, there is a new diffraction peak at 22.5° (2θ) appeared in QPSF, which

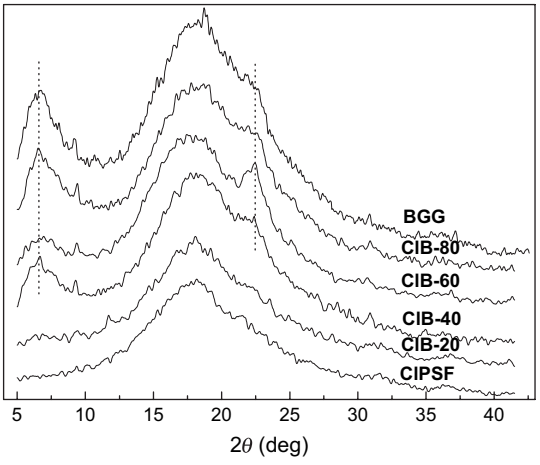

Fig. 11. WAXD diffraction patterns of the ClB blends.

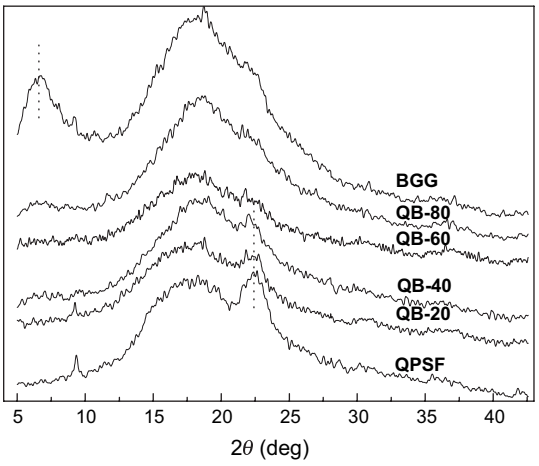

Fig. 12. WAXD diffraction patterns of the QB blends.

indicates that QPSF has higher crystallization than ClPSF. It can be explained that the polycationic quaternized groups repulse each other in the aromatic rings, which causes polysulfone chains to stretch orderly and crystallize easily. If QPSF and BGG have low compatibility then each polymer would have its own crystal region in the blends, and the WAXD patterns of the samples would be expressed as simply mixed patterns of the two polymers. However, when BGG is introduced into QPSF matrix, the crystallization of QPSF is destroyed. The intensity of diffraction at 22.5° decreases with an increase of BGG content from 20 to 40 wt%. When BGG content further increases, the crystallization peak at 22.5° disappears completely. The diffuse scattering near 6.5°, ascribed to BGG, does not appeared in the blends, which indicates that the crystallization of BGG is also destroyed. The change of the patterns indicates that a strong intermolecular interaction occurred between the two polymers, and destroyed the original crystalline domains of QPSF and BGG. The outcome, deduced from WAXD, is consistent with that of FTIR and DSC.

3.3. Mechanical properties of the blends

3.3.1. Mechanical properties of the ClB and QB blends

It is known that the interaction between polymers should influence the mechanical properties of the blend polymer. The mechanical properties of immiscible blends are sometimes worse than that of their component polymers because of the lack of interfacial adhesion between the components [42]. The dependency of the tensile strength and elongation at break on BGG content for the ClB blends is shown in Fig. 13. ClPSF shows the characteristic of plastic polymers, and the tensile strength and elongation at break are 40.7 MPa and 6.1%, respectively. The values of tensile strength and elongation at break of BGG are much smaller than that of ClPSF. For the blends, the tensile strength decreases with increasing BGG content and reaches 25.1 MPa at 80 wt% content of BGG. Simultaneously, the change of elongation at break is similar to that of the strength, and the maximum value of

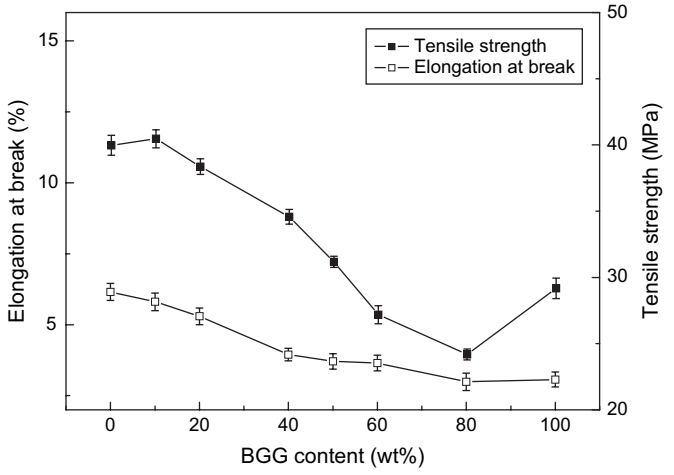

Fig. 13. Tensile strength and elongation at break of the ClB blends as a function of BGG content.

2.9% is reached when the content of BGG is 80 wt%. The resulting blends exhibit rapid decrease in tensile strength and elongation at break, due to some phase separation as proved by DSC and SEM.

Tensile strength and elongation at break of the QB blends as a function of BGG content are shown in Fig. 14. The characterization discussed above indicates miscibility between the two polymers in the blends. Tensile properties can provide an answer to this question. The tensile strengths of the blends change with an increase of BGG content, and the maximum value of 44.1 MPa is reached when the content of BGG is 60 wt%. The change of elongation at break is similar to that of the strength, and the maximum value of 15.5% is reached when the content of BGG is 20 wt%. The conclusion can be drawn that BGG introduced into QPSF matrix has considerably improved the mechanical properties of the blends, and the enhancement of tensile strength may be due to the strong interaction between QPSF and BGG, which gives rise to an intermolecular complex or the physical crosslinkage.

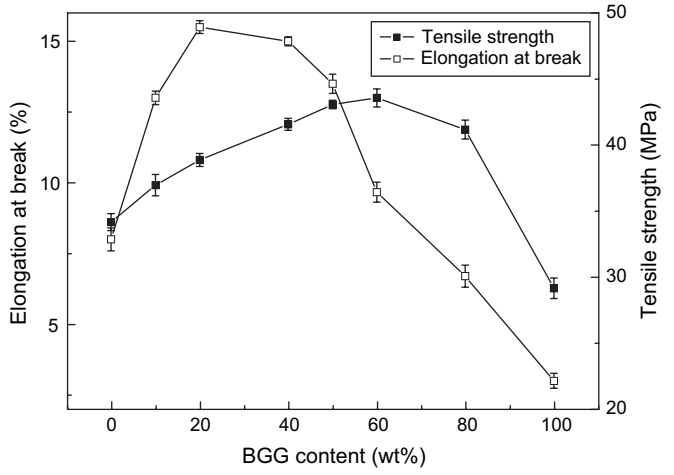

Fig. 14. Tensile strength and elongation at break of the QB blends as a function of BGG content.

Table 5
Tensile strength and elongation at break of QB-20 blend at different RH

RH (%)	Moisture content (wt%)	Tensile strength (MPa)	Elongation at break (%)
0	0.02	50.5 ± 0.6	2.1 ± 0.1
10	0.54	49.2 ± 0.4	6.5 ± 0.5
20	2.41	47.7 ± 0.3	8.2 ± 0.3
32	4.56	45.1 ± 0.5	12.6 ± 0.4
42	6.48	40.4 ± 0.3	14.5 ± 0.2
52	7.46	37.5 ± 0.3	15.5 ± 0.2
66	8.56	36.8 ± 0.2	16.3 ± 0.3
75	9.43	37.4 ± 0.4	15.6 ± 0.2
86	9.85	39.1 ± 0.3	14.1 ± 0.3
98	10.21	40.2 ± 0.5	13.7 ± 0.2

3.3.2. Effect of moisture content on mechanical properties of the QB blends

The moisture absorbed in the membranes can act as plasticizer, leading to a change in the microstructure and mechanical properties of the membranes. Therefore, the RH value of ambient atmosphere is an indispensable factor for the manufacture, characterization, store and use of QPSF-based materials. Tensile strength and elongation at break of QB-20 blend at different RH are shown in Table 5. It can be seen that the tensile strength decreases to a minimum value when RH value reaches 60%. After that the tensile strength tends to increase slightly with RH value. The decrease in tensile strength at low moisture content may be caused by the formation of hydrogen bonding between water molecules and BGG. With the presence of moisture, this hydrogen bonding is broken and new hydrogen bonding with water molecules is then formed, which causes a decrease in the mechanical properties of the natural polymer–synthesized polymer composites [43]. The increase in tensile strength at high moisture content probably involved swelling of the BGG and a reduction in interfacial gaps between QPSF and BGG. According to the reports by Karmaker et al. [44], high amount of water could cause swelling of the fiber which filled the gaps between the fiber and polymer matrix and eventually led to an increase in the mechanical strength of the composites. The elongation at break of QB-20 blend is also shown in Table 5. It was found that the elongation at break increases with moisture content to give a maximum before decreasing at higher moisture content. The increase in elongation is due to the lubrication effect of the presence of moisture, which allows the polymer chains to slip past each other. The decrease in elongation at high moisture content is caused by BGG swelling which filled in the gaps between BGG and QPSF matrix, as described earlier.

4. Conclusions

A series of blends were prepared from BGG and QPSF (10–80 wt%) or ClPSF (10–80 wt%) by blending in solution. The results from FTIR, SEM, AFM, DSC and WAXD measurements revealed that typical phase separation existed in the ClB blends containing ClPSF with chloromethylated groups. Interestingly, good or certain miscibility over the

entire composition ratio of QPSF to BGG existed in QB blends containing QPSF with quaternized groups, which was attributed to stronger interfacial attraction and better phase mixing as a result of the relatively stronger inter- and intra-molecular hydrogen bonding and the specific electrostatic interaction between QPSF and BGG. The introduction of BGG into QPSF matrix can improve greatly the mechanical properties of the blends. Compared with pure QPSF blend, the blends show improved mechanical strength, and the maximum value of 44.1 MPa was reached when BGG content was 60 wt%. Furthermore, the mechanical properties of QB-20 blend at different RH value are also discussed. It was found that the composite properties changed considerably with moisture content. Therefore, the quaternized groups in PSF derivatives play a very important role in the improvement of the miscibility between QPSF and BGG.

References

[1] Devia N, Manson JAM, Sperling LH. Macromolecules 1979;12:360.
[2] Cheng Y, Brown KM, Prud'homme RK. Biomacromolecules 2002;3:456.
[3] Wientjes RHW, Duits MHG, Jongschaap RJJ, Mellema J. Macromolecules 2000;33:9594.
[4] Arvanitoyannis I. J Macromol Sci Rev Macromol Chem Phys 1999;C39:205.
[5] Liu Y, Shao Z, Zhou P, Chen X. Polymer 2004;45:7705.
[6] Çaykara T, Demirci S, Eroğlu MS, Güven O. Polymer 2005;46:10750.
[7] Lu Y, Zhang L, Zhang X, Zhou Y. Polymer 2003;44:6689.
[8] Cao XD, Zhang L. J Polym Sci Part B Polym Phys 2005;43:603.
[9] Huang J, Zhang L. Polymer 2002;43:2287.
[10] Zhou Q, Zhang L, Zhang M, Wang B, Wang S. Polymer 2003;44:1733.
[11] Zhang L, Zhou Q. J Polym Sci Part B Polym Phys 1999;37:1623.
[12] Guiver MD, Robertson GP, Foley S. Macromolecules 1995;28:7612.
[13] Ghosal K, Chern RT, Freeman BD, Daly WH, Negulescu II. Macromolecules 1996;29:4360.
[14] Charoensirisomboon P, Saito H, Inoue T, Weber M, Koch E. Macromolecules 1998;31:4963.
[15] M'Bareck CO, Nguyen QT, Alexandre S, Zimmerlin I. J Membr Sci 2006;278:10.
[16] Louis C, Chailan JF, Bartolomeo P, Vernet JL. Polymer 2001;42:7107.
[17] Hwang WJ, Cho K, Park CE, Huh W. J Appl Polym Sci 1999;74:33.
[18] Wei YM, Xu ZL, Qusay FA, Wu K. J Appl Polym Sci 2005;98:247.
[19] Gonzalo GE, José I, Jon N. Macromol Mater Eng 2005;290:38.
[20] Niranjan MP, David WD, James LH, Dean CW, James EM. Macromolecules 1988;21:2689.
[21] Han MJ, Nam ST. J Membr Sci 2002;202:55.
[22] Deimede V, Voyiatzis GA, Kallitsis JK, Qingfeng L, Bjerrum NJ. Macromolecules 2000;33:7609.
[23] Coleman MM, Zarian J. J Polym Sci Polym Phys Ed 1979;17:837.
[24] Ng CWA, MacKnight WJ. Macromolecules 1996;29:2412.
[25] Lu X, Weiss RA. Macromolecules 1991;24:4381.
[26] Lu X, Weiss RA. Macromolecules 1992;25:6185.
[27] Liu C, Xiao CB. J Appl Polym Sci 2004;93:1868.
[28] Avram E. Polym Plast Technol Eng 2001;40:275.
[29] Haslan J, Hamilton B, Squirell DM. Analyst 1960;86:556.
[30] Sugiyama N, Shimahara H, Andoh T, Takemoto M, Kamata T. Agric Biol Chem 1972;36:1381.
[31] Hsieh TT, Hsieh KH, Simon GP, Tiu C, Hsu HP. J Polym Res 1998;5:153.
[32] Park JW, Im SS. Polymer 2003;44:4341.
[33] Biliaderis CG, Lazaridou A, Arvanitoyannis I. Carbohydr Polym 1999;40:29.
[34] Bikiaris D, Prinos J, Botev M, Betchev C, Panayiotou C. J Appl Polym Sci 2004;93:726.
[35] Brannock GR, Barlow JW, Paul DR. J Polym Sci Part B Polym Phys 1991;29:413.
[36] Fox TG. Bull Am Phys Soc 1956;1:123.
[37] Gordon M, Taylor JS. J Appl Chem 1952;2:495.
[38] Kwei TK. J Polym Sci Polym Lett Ed 1984;22:307.
[39] Belorgey G, Prud'homme RE. J Polym Sci Polym Phys Ed 1982;20:191.
[40] Belorgey G, Aubin M, Prud'homme RE. Polymer 1982;23:1051.
[41] Lai WC, Liau WB, Lin TT. Polymer 2004;45:3073.
[42] Paul DR, Barlow JW. J Macromol Sci Rev Macromol Chem 1980;C18:109.
[43] Sombatsompop N, Chaochanchaikul K, Phromchirasuk C, Thongsang S. Polym Int 2003;52:1847.
[44] Karmaker AC, Hoffmann A, Hinrichsen G. J Appl Polym Sci 1994;54:1803.